Benzene and NO_x photocatalytic assisted removal using indoor lighting conditions

DM Tobaldi,[a,b,*] D Dvoranová,[c] L Lajaunie,[d,e] K Czikhardtová,[c] B Figueiredo,[f] MP Seabra,[b] JJ Calvino,[d,e] JA Labrincha[b]

[a] *CNR Nanotec, Institute of Nanotechnology, Campus Ecoteckne, 73100 Lecce, Italy*

[b] *Department of Materials and Ceramic Engineering and CICECO–Aveiro Institute of Materials, University of Aveiro, Campus Universitário de Santiago, 3810–193 Aveiro, Portugal*

[c] *Institute of Physical Chemistry and Chemical Physics, Faculty of Chemical and Food Technology, Slovak University of Technology in Bratislava, Radlinského 9, Bratislava, SK-812 37, Slovak Republic*

[d] *Departamento de Ciencia de los Materiales e Ingeniería Metalúrgica y Química Inorgánica, Facultad de Ciencias, Universidad de Cádiz, Campus Río San Pedro S/N, Puerto Real 11510, Cádiz, Spain*

[e] *Instituto Universitario de Investigación de Microscopía Electrónica y Materiales (IMEYMAT), Facultad de Ciencias, Universidad de Cádiz, Campus Río San Pedro S/N, Puerto Real 11510, Cádiz, Spain*

[f] *Graphenest, Lugar da Estação, Edifício Vouga Park, 3740–070 Paradela do Vouga, Portugal*

KEYWORDS: Photocatalytic VOC and NO_x removal; Indoor lighting; Indoor air quality; Smart-materials; Graphene decorated titania.

*Corresponding author.

E-mail addresses: **david.tobaldi@nanotec.cnr.it**; **david@davidtobaldi.org** (DM Tobaldi)

Twitter: **@D14MT** (DM Tobaldi)

Abstract

Modern life-style is creating an *indoor generation*: human beings spend approximately 90% of their time indoors, almost 70% of which is at home – this trend is now exacerbated by the lockdowns/restrictions imposed due to the COVID-19 pandemic. That large amount of time spent indoors may have negative consequences on health and well-being. Indeed, poor indoor air quality is linked to a condition known as sick building syndrome. Therefore, breathing the freshest air possible it is of outmost importance. Still, due to reduced ventilation rates, indoor air quality can be considerably worse than outdoor. HVAC, air filtration systems and a well-ventilated space are a partial answer. However, these approaches involve only a physical removal. Photocatalytic mineralisation of pollutants into non-hazardous, or at least less dangerous compounds, is a more viable solution for their removal. Titanium dioxide, the archetype photocatalytic material, needs UVA light to be "activated". However, modern household light emitting diode lamps irradiate only in the visible region of the solar spectrum. In this short-communication, we show that the surface of titanium dioxide nanoparticles modified with copper oxide(s) and graphene shows promise as a viable way to remove gaseous pollutants (benzene and NO_x) by using a common light emitting diode bulb, mimicking real indoor lighting conditions. Titanium dioxide, modified with 1 mol% Cu_xO and 1 wt% graphene, proved to have a stable photocatalytic degradation rate, three times higher than that of unmodified titania. Materials produced in this research work are thus strong candidates for offering a safer indoor environment.

1. Introduction

Human-beings spend 90% of their time indoor, approximately 70% of this time being spent at home [1]. Indoor air quality (IAQ) is referred to as: "*the quality of the air in a home, school, office, or other building environment*" [2]. According to the United States Environmental Protection Agency, IAQ potential impact on human health can be significant. Indeed, long-term exposure to air pollution [mostly given by nitrogen oxides (NO_x), and volatile organic compounds (VOCs)] has serious health effects. It has been shown that this can eventually lead to premature mortality [3]. Variegated are the sources of indoor pollution: combustion, cleaning supplies, and the building materials themselves [2]. Lockdowns/restrictions imposed by Governments during the (ongoing, at the time of writing) COVID-19 pandemic on the one hand resulted in less industrial, and in general, outdoor emissions. However, this situation led to an (unrequested) increase of the time we stay home, thus to a non-negligible worsening of the IAQ. This in turn led to negative health outcome on human-beings during the COVID-19 lockdowns [4].

Possible answers to reduce and remove air pollutants, besides spending more time outdoor, are: adsorption, electrochemical oxidation processes and filtration [5]. However, those technologies involve physical removal (therefore, requiring replacement), cleaning, and disposal of any consumable. Mineralisation of those

pollutants into non-hazardous, or at least less hazardous compounds by means of photocatalysis is of great promise as a more feasible solution for their removal [6]. Amongst the semiconductor materials used as photocatalysts, titanium dioxide (TiO_2, titania), is still the most promising to remove harmful gases – Earth-abundant, high oxidising power and resistance to photocorrosion, non-toxic, and cost-effective material. However, being a wide-gap semiconductor, TiO_2 needs UVA light for the photocatalytic phenomenon to be exploited on its surface [7]. This goes against the usual lighting used indoors: lamps emitting in the visible region of the solar spectrum. Furthermore, a recent directive of the European Union states that light emitting diodes (LEDs) bulbs, emitting with no UV lines, should replace fluorescent and/or incandescent lamps as household room illumination systems [8]. Indeed, there are advantages of LED technology over the classical light irradiation sources: they do contain no Hg, they have higher energy efficiency, and have longer life-time [9]. Thus, the need to modify titania's surface for this to absorb visible light, and being active under real indoor household conditions, is concrete. Indeed, most of the previous research about photocatalysis and visible-light deal with halogen or xenon arc lamps [10], are not compatible with those used in an actual indoor environment. Little work has been carried out using common household visible-LEDs so far, the majority of the research dealing with organic dyes decolourisation. Ferrari-Lima and colleagues tested the photocatalytic activity of N-doped TiO_2 and ZnO in aqueous solutions containing benzene, toluene and xylenes using a white LED lamp [11]. Douven and co-workers used a near-visible LED light (emission at 395 nm) and TiO_2 co-doped with nitrogen and iron for the degradation of an organic dye in the liquid-solid phase [12]. A low power LED bulb and sulfur-doped TiO_2 were used to decolour an organic dye solution [13]. Yet, Vaiano and *et al*. showed that N-doped TiO_2 modified with organic up-conversion phosphors was able to decolour a number of organic dyes in aqueous suspension using white LEDs [14]. [It has to be stressed that these latter works are not the ideal systems to show visible-light photocatalytic activity, as photosentisitation effects may happen [15].] A very recent work by Eimer *et al*. showed that mesoporous nanostructured TiO_2 co-doped with iron and carbon was effective in the photocatalytic degradation of ibuprofen using visible-LED modules [16].

To fill that literature gap, we show that surface co-modification of TiO_2 with graphene and copper oxide(s) (Cu_xO) is a promising way to photocatalytically remove benzene and nitrogen oxides (NO_x) from the gas-phase using a white LED bulb typically used in households. In particular, we highlight that 1 mol% copper and 1 wt% graphene gave TiO_2 a stable visible-light induced photocatalytic activity, three times higher than that of unmodified titania, and of a carbon-modified commercial anatase too. Copper oxide(s) behaves as visible-light absorber, while graphene enhances the space charge separation of the photogenerated exciton in that hybrid TiO_2-based composite. Our material shows therefore potential as an additive to building materials for interior use to improve IAQ.

2. Results and discussion

2.1 Microstructural and optical information

As described in the *Experimental Section* reported in the Supporting Information material, hybrid copper oxide(s) and graphene TiO_2 nanoparticles were synthesised following an aqueous sol-gel method [15]. Microstructure and crystallographic properties are discussed in detail in [17]. Briefly, X-ray powder diffraction (XRPD) analyses showed that copper ions did not enter TiO_2 structure. However, together with graphene, they hindered the anatase-to-rutile phase transition (ART), and the nucleation and growth of both anatase and rutile crystalline domains [17]. Indeed, we previously showed that unmodified TiO_2 thermally treated at 250 °C / 8h consisted of 92.8 wt% anatase, 5.1 wt% rutile, and 2.1 wt% brookite. Anatase fraction increased to 94.4 wt%, and 95.5 wt% in **Cu-G0.5/250**, and **Cu-G1.0/250**, respectively. Anatase crystalline domains in unmodified TiO_2 were shown to have an average diameter of 4.4 nm, those of rutile 8.7 nm. The addition of copper and graphene led to a smaller size of anatase's domains, being around 3 nm in **Cu-G0.5/250**, and **Cu-G1.0/250**, respectively.

The increase in the maximum firing temperature to 450 °C favoured the ART: anatase fraction in unmodified TiO_2 was 70.8 wt%, whilst rutile accounted for 19.5 wt%, brookite 9.7 wt%. Yet, copper oxide(s) and graphene modifications delayed the ART. Anatase fraction increased to 89.6 wt% (rutile being 8.6 wt%), and 89.0 wt% (with a rutile fraction equal to 9.8 wt%) in **Cu-G0.5/450**, and **Cu-G1.0/450**, respectively. Anatase and rutile diameters in unmodified TiO_2 were 8.7 nm, and 14.4 nm, respectively. Those in **Cu-G0.5/450**, and **Cu-G1.0/450** decreased to around 7 nm and 9 nm for anatase and rutile, respectively [17]. XRPD analyses data are listed in Table S1 of the Supporting Information material. Figure 1 shows the TEM study performed on the sample **Cu-G1.0/250.** The STEM-ADF micrograph (Figure 1a) shows the superposition of the graphene flake and nanoparticles in the same area. The size of the flakes is typically between 500 and 1000 nm. The corresponding EELS analysis is shown in Figure 1b. The EELs spectra acquired on the graphene flake shows only the presence of the C−*K* edge, and no edges related to O, Ca and N could be observed in the same spectral range. In addition, the C−*K* edge present characteristic fine structures of carbon materials with a high sp^2 content [18]. As expected, the EELS spectra acquired on the nanoparticle supported by the graphene flake show the presence of the Ti−$L_{2,3}$ and O−*K* edges in addition of the C−*K* edges. Figure 1c shows a HR-TEM micrograph acquired on the graphene flake, displaying the high crystalline quality of the flake. Automatic indexation of the corresponding FFT (inset of Figure 1c) shows that this belongs to the graphitic basal plane seen along the [001] zone axis. Figure 1d displays a HR-TEM micrograph acquired on TiO_2 nanoparticles. The nanoparticles have a sub-spherical morphology with diameter typically between 5 and 10 nm.

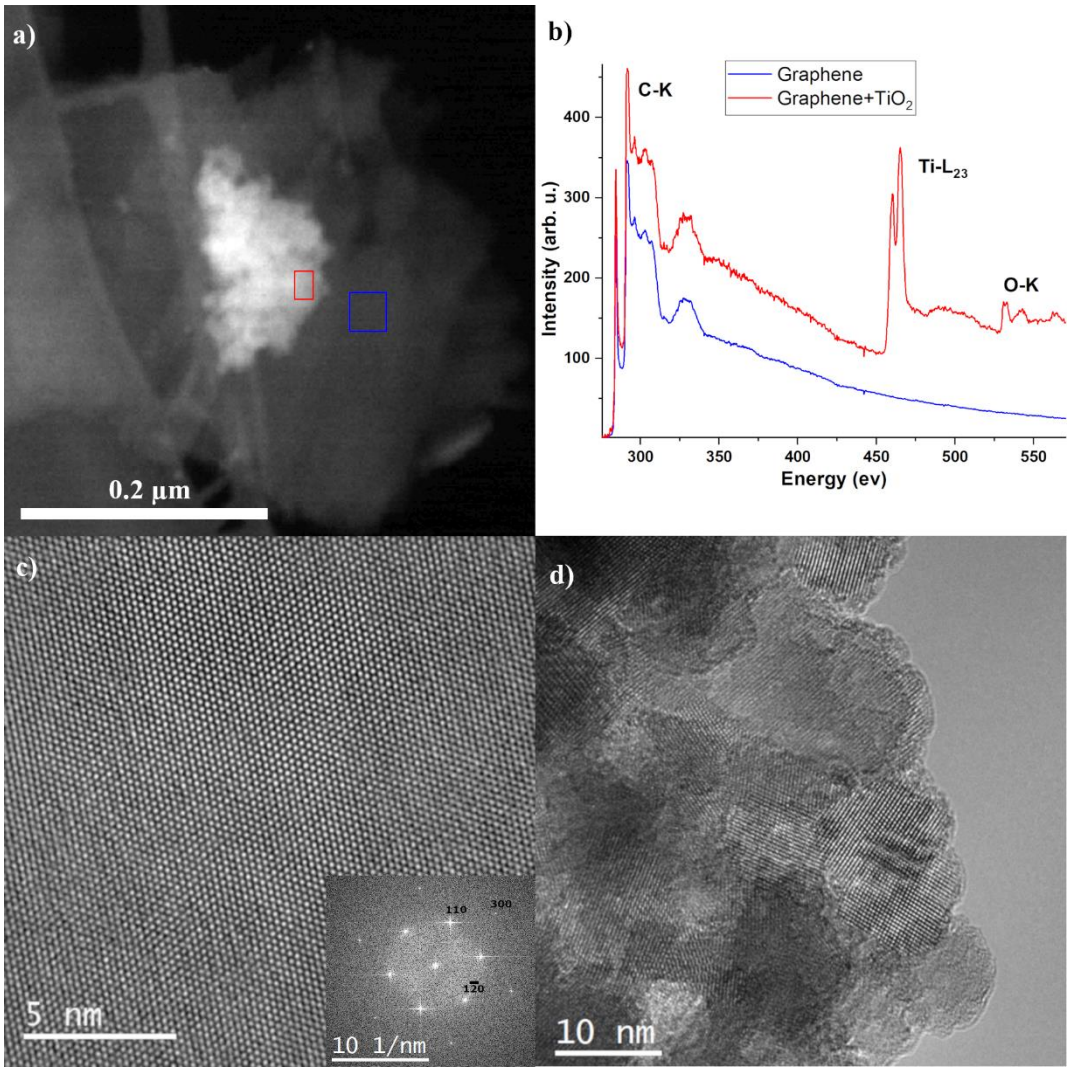

Figure 1. Transmission electron microscopy analysis of the sample **Cu-G1.0/250**. a) STEM-ADF micrograph. The red and blue squares highlight the areas used for the acquisition of the corresponding blue and red EELS spectra shown on the right. b) EELS spectra acquired on the graphene flake, and on the graphene plus TiO_2 nanoparticles area. c) Filtered HR-TEM image of the graphene flake. The inset shows the corresponding FFT pattern. **c**) HR-TEM image of TiO_2 nanoparticles.

Optical spectra of **K7000** and those of unmodified TiO_2 are shown in Figure S2. They show a single absorption band at around 3.2 eV, which is assigned to the band-to-band transition in TiO_2 [19]. Addition of graphene and copper oxide(s) gave titania further optical features, as displayed in Figure 2. As also previously shown in [17], the strong band centred at approximately 1.5 eV is assigned to *d*–*d* electronic transitions in Cu^{2+} [20]; the absorption feature at around 2.75 eV belongs to interfacial charge transfer (IFCT). This is an electron transferring from the valence band of TiO_2 to both the copper oxide(s) and graphene clusters that are grafted at the interface with titania [21,22]. We have previously proven that those latter specimens exhibited (reversible) photochromism when irradiated by a white light LED lamp [17]. [This was the same visible white LED lamp as that employed in those photocatalytic experiments. 5.0 $mW.cm^{-2}$ was the radiant flux in the photochromic experiments; 5.8 $mW.cm^{-2}$ that in the gas-phase photocatalytic experiments.] However, while photochromism in specimens thermally treated at 250 °C / 8h was mainly due to IFCT (Figure 2a), the P-type

change in colour observed in samples treated at 450 °C / 2 h was a visible-light induced photocatalytic colour switching. That is: the photogenerated electron in titania's conduction band was able to continuously reduce Cu(II) to Cu(I). This is better shown in Figure 2b: at around 30 min irradiation time an absorption feature centred at ~2.25 eV, and belonging to the band-to-band transition of newly formed Cu_2O [23], appeared. After 300 min visible light irradiation time, the optical features due to IFCT and Cu^{2+} *d*–*d* transitions completely disappeared in favour of that belonging to Cu_2O. This behaviour influenced the apparent optical band-gap (E_g) of the Cu_xO-graphene modified titania-based materials, Table 1 and Table S2.

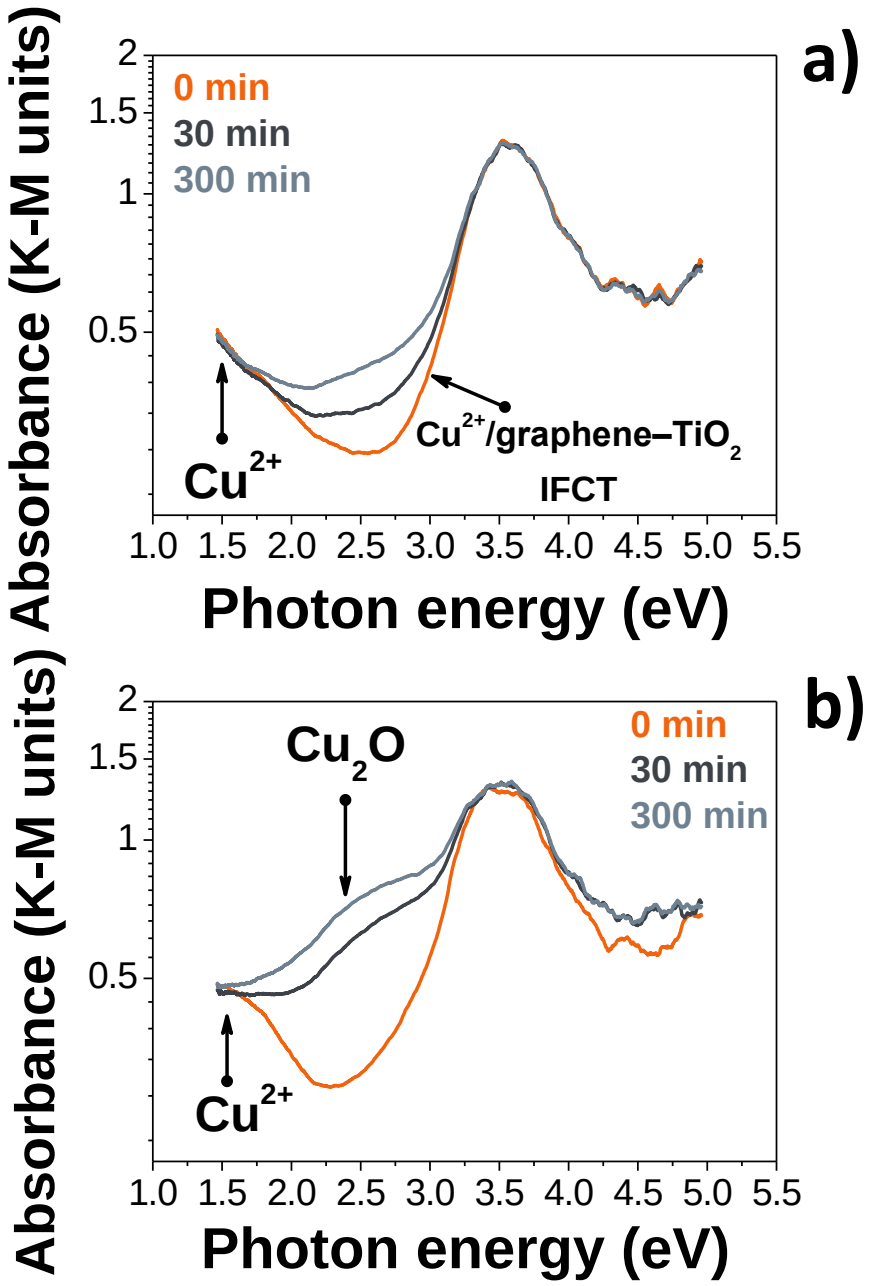

Figure 2. Pseudo-absorption spectra [absorbance, in Kubelka-Munk (K-M) units, *versus* photon energy] of: a) fresh **Cu-G1.0/250**, after 30, and 300 min visible light LED irradiation. b) Fresh **Cu-G1.0/450**, after 30, and 300 min visible light LED irradiation. The radiant flux per unit area reaching the surface of the specimens was 5.0 $mW.cm^{-2}$ in the visible spectral region. Modified from [17].

Table 1 – Apparent optical E_g of fresh and irradiated specimens (hybridised with 1 wt% graphene and 1 mol% Cu), estimated according the Tauc procedure. The absolute error in the Tauc plot measurements was ≤ 1%.

Sample	Visible-light LED irradiation time, min	Apparent optical band-gap, eV	
		Direct	Indirect
Cu-G1.0/250	0	**3.12**	2.55
	30	**3.11**	2.52
	300	**3.09**	2.44
Cu-G1.0/450	0	**3.03**	2.54
	30	**2.95**	2.16
	300	**2.91**	1.99

Anatase is reported to have an indirect E_g transition, while rutile a direct band-to-band transition [24]. However, our specimens are composed of mixed anatase-to-rutile wt% ratios (*cf* Table S1). To them, the direct *E*g transition model would suit better [25]. Given this scenario, the apparent optical direct E_g of specimens thermally treated at 250 °C / 8h does not significanty vary with the irradiation time. On the other hand, the apparent direct E_g of specimens thermally treated at 450 °C / 2h experienced a red-shift upon visible-light irradiation, as listed in Tables 1, and Table S2, enabling visible-light absorption. [This does not necessarily correspond to an actual rigid narrowing of TiO_2's E_g, but it might be the consequence of some electronic transitions deriving from intra-gap localised levels.]

The indirect technique of electron paramagnetic resonance (EPR) spectroscopy has been employed to examine the role of photogenerated electrons in the studied reacting systems. To this aim, methylviologen dication MV^{2+}, a viologen derivative, has been employed. As it is a well-known electron scavenger [26], its reduction from diamagnetic MV^{2+} to paramagnetic $MV^{\bullet+}$ radical anion can be monitored by EPR spectroscopy. Figure 3 displays the relative concentration of EPR spectra (presented as the area of EPR signals) of $MV^{\bullet+}$ radical cation generated upon LED@365 nm exposure in the dimethylsulfoxide (DMSO) dispersion under an inert atmosphere. The highest signal was detected in **Ti/450**. However, the generation of $MV^{\bullet+}$ radical cation in the reacting system with Cu_xO and Cu_xO-graphene modified titania-based materials was significantly lower. In the **Cu/450**, **Cu-G0.5 /450,** and **Cu-G1.0/450** systems the photogenerated electron migration from the conduction band of TiO_2 to the conduction band of CuO is favourable, the reduction of Cu(II) to Cu(I) occurs as a consecutive reaction. The lowest signal was detected in **Cu-G0.5 /450**, which correlates well with our previous data, in which the system with TiO_2 and 0.5 wt% graphene preferred the kinetics of Cu(II) reduction [17]. It has to be noted that reduction has been performed here under an inert atmosphere, to avoid consecutive reactions of a photogenerated electron with molecular oxygen, as well as the broadening of the EPR signal due to spin-spin interaction with an oxygen molecule.

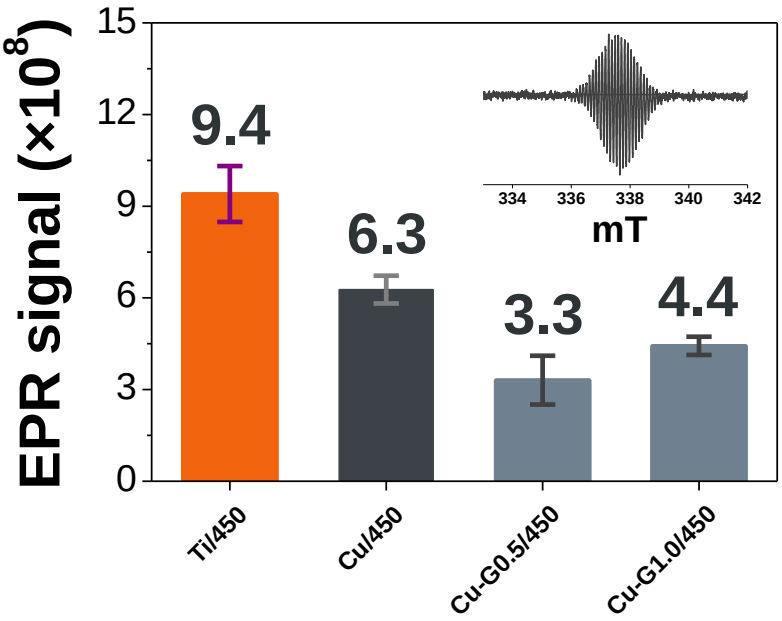

Figure 3. Area of EPR spectra of radical cation MV^{2+} measured upon LED@365 exposure (dose 2.7 $J.cm^{-2}$) in dimethylsulfoxide (DMSO) suspensions of photocatalyst under inert atmosphere. Initial concentration of photocatalyst was 0.67 $mg.mL^{-1}$, and MV^{2+} 0.65 mM. Inset reports the experimental EPR spectrum of radical cation $MV^{\bullet+}$ measured upon exposure (magnetic sweep width = 12 mT) with spin Hamiltonian parameters obtained from the simulation analysis: a_N(2N) = 0.396 mT, a_H(6H) = 0.355 mT, a_H(4H) = 0.098 mT, a_H(4H) = 0.127 mT; g = 2.0030.

The photoinduced electron transfer has been also examined in the aqueous system of radical cation $ABTS^{\bullet+}$, which can be reduced to parent diamagnetic molecule ABTS. (Figure 4) This process may be monitored *via* electron absorption spectroscopy due to the presence of selective absorption bands at 735 nm and 415 nm, well distinguishable from the absorption maxima of its reduced ABTS (340 nm) and oxidised $ABTS^{2+}$ (518 nm) forms [27]. Light exposure led to a decrease in the absorption maxima at 735 nm and 415 nm, together with an increase of that centred at 340 nm. For the system containing **G1.0/450** (Figure 4a) and **Ti/450** within 20-minute exposure, the blue-green colour suspension of $ABTS^{\bullet+}$ changed to a slight yellow one, which represents the ABTS form. Thus, the change in colour indicates the effective photoreduction of the radical cation $ABTS^{\bullet+}$. The presence of Cu_xO and Cu_xO-graphene modified titania-based material in the aqueous $ABTS^{\bullet+}$ system caused a decreased rate in photoreduction, due to consecutive reaction of photogenerated electrons (Figure 4b). In the irradiated aqueous titania dispersions, not only radical cation $ABTS^{\bullet+}$ is reduced to ABTS *via* photo-electrons, but also *via* the superoxide radical anions, generated by the reaction of molecular oxygen with the photo-electrons. Despite the stability of superoxide radical anions in a protic solvent as DMSO, their reaction with photons in aqueous solutions is favourable, and hydrogen peroxide, which can be further involved in photocatalytic processes, is being formed [27,28]. Based on the obtained results under given experimental conditions, we suppose that the photoreduction of radical cation $ABTS^{\bullet+}$ prevailed in the system with **Ti/450**. However, the behaviour of reacting systems **Cu/450**, **Cu-G0.5 /450**, and **Cu-G1.0/450** with $ABTS^{\bullet+}$ upon exposure differs, and the reaction rate of the $ABTS^{\bullet+}$ photoreduction is lower

due to consecutive reduction of Cu(II) to Cu(I). As was mentioned above, hydrogen peroxide may be formed, so a Fenton-like reaction in aqueous suspensions can be considered, and the reversible Cu(II) formed could again be introduced for being reduced. Despite the anticipated, rather complex mechanism, the results obtained correlates well with the proposed photoinduced electron transfer to the CuO conduction band upon exposure.

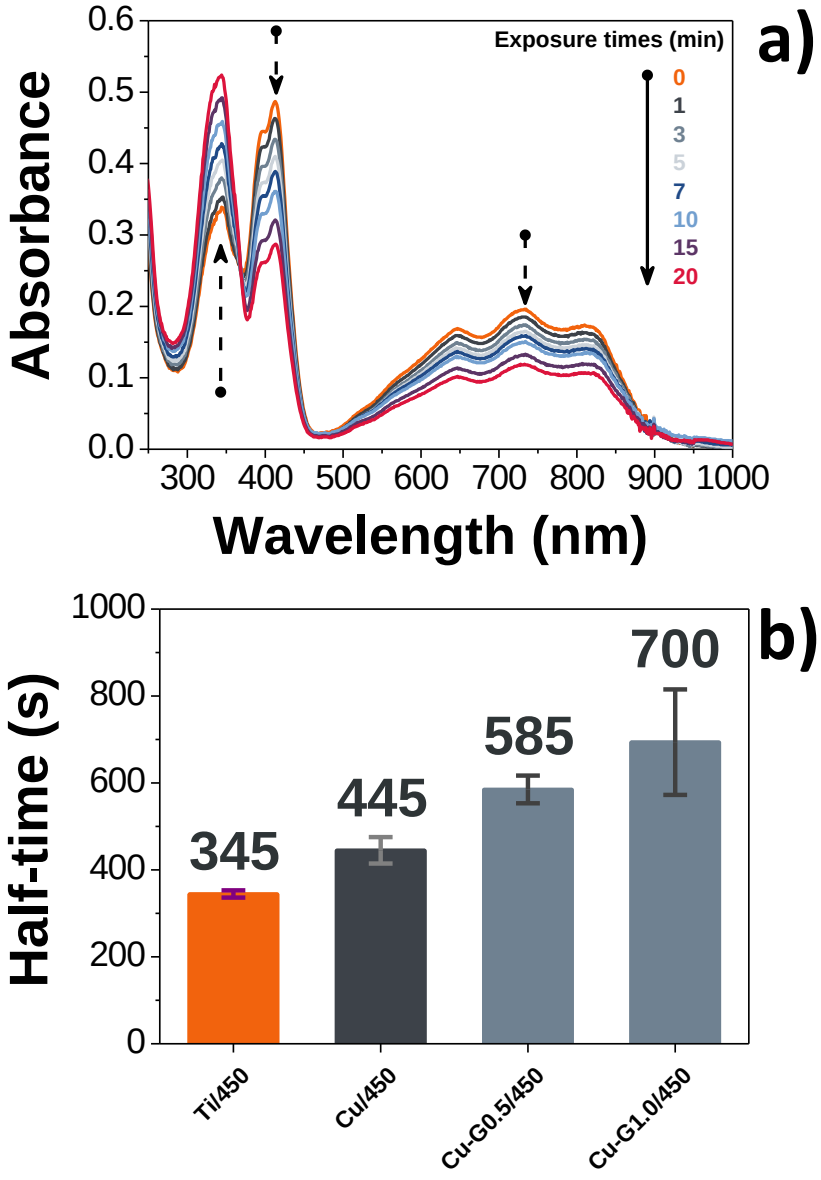

Figure 4. Time-course of electronic absorption spectra of $ABTS^{\bullet+}$ radical cation monitored in intervals during 20-minute LED@365 nm exposure in the aerated aqueous suspension of **Cu-G1.0/450**. (b) Half-times of photoreduction of $ABTS^{\bullet+}$ in titania dispersions. Initial concentration of photocatalyst was 0.10 $mg.mL^{-1}$ and $ABTS^{\bullet+}$ 15 µM; optical path length was 1 cm.

2.2 Photocatalytic gas-solid phase results

2.2.1 Benzene removal

Visible-light induced benzene removal results, reported as FQE and k'_{app} (first 1 h reaction time), are shown in Figure 5. All of the samples were shown to be photocatalytically active, with specimens thermally treated at the higher temperature displaying higher photocatalytic activity. TiO_2 specimens modified with copper oxide(s) and graphene thermally treated at 250 °C / 8h showed a lower photocatalytic activity compared to the control specimens (*i.e.* **Ti/250**, and **K7000**). This might be justified by copper being still in its cupric (Cu^{2+}) oxidation state, therefore CuO, as described above. Indeed, in such an alignment, the interface between TiO_2 and CuO is organised as a straddling gap (type-I) heterojunction, thus favouring a recombination of the photogenerated exciton (Figure 6a).

On the other hand, specimens thermally treated at 450 °C / 2h all showed higher visible-light photocatalytic activity than unmodified TiO_2, and commercial **K7000** anatase. Specimens hybridised with 1 mol% Cu, and 0.5 and 1.0 wt% graphene (*i.e.* **Cu-G0.5/450**, and **Cu-G1.0/450**) possessed FQE rates equal to 21.9, and 30.6×10^{-10} molecules.photon^{-1}, respectively. Those values are, respectively, around three and four times higher than that of **Ti/450** (FQE = 6.9×10^{-10} molecules.photon^{-1}), Figure 5c. This is well confirmed by the first hour reaction time k'_{app} values, reported in Figure 5d: **Ti/450** had an initial k'_{app} value equal to 1.6×10^{-2} h^{-1}. Those of **Cu-G0.5/450**, and **Cu-G1.0/450** were: 3.1, and 4.5×10^{-2} h^{-1}, respectively.

The optical behaviour of those latter hybridised specimens (**Cu-G0.5/450**, and **Cu-G1.0/450**) upon visible-light irradiation is quite different, as shown in Figure 2b. In them, photocatalytic induced photochromism made a swift and continuous reduction of Cu(II) to Cu(I) possible, leading to a regular red-shift in the E_g upon visible-light irradiation. Then, the interface between TiO_2 and Cu_2O is aligned as a staggered gap (type-II) heterojunction, thus favouring a spatial charge separation of the photogenerated exciton (Figure 6b). Besides, graphene in the hybrids allowed for an increase in both electric transport and thermal conductivity [17,29]. This is thermodynamically favourable, as graphene work function (WF) is at 4.5 eV (with respect to the vacuum level) [30]. This explains the visible-light induced photocatalytic activity of TiO_2 specimens modified with Cu_xO and graphene.

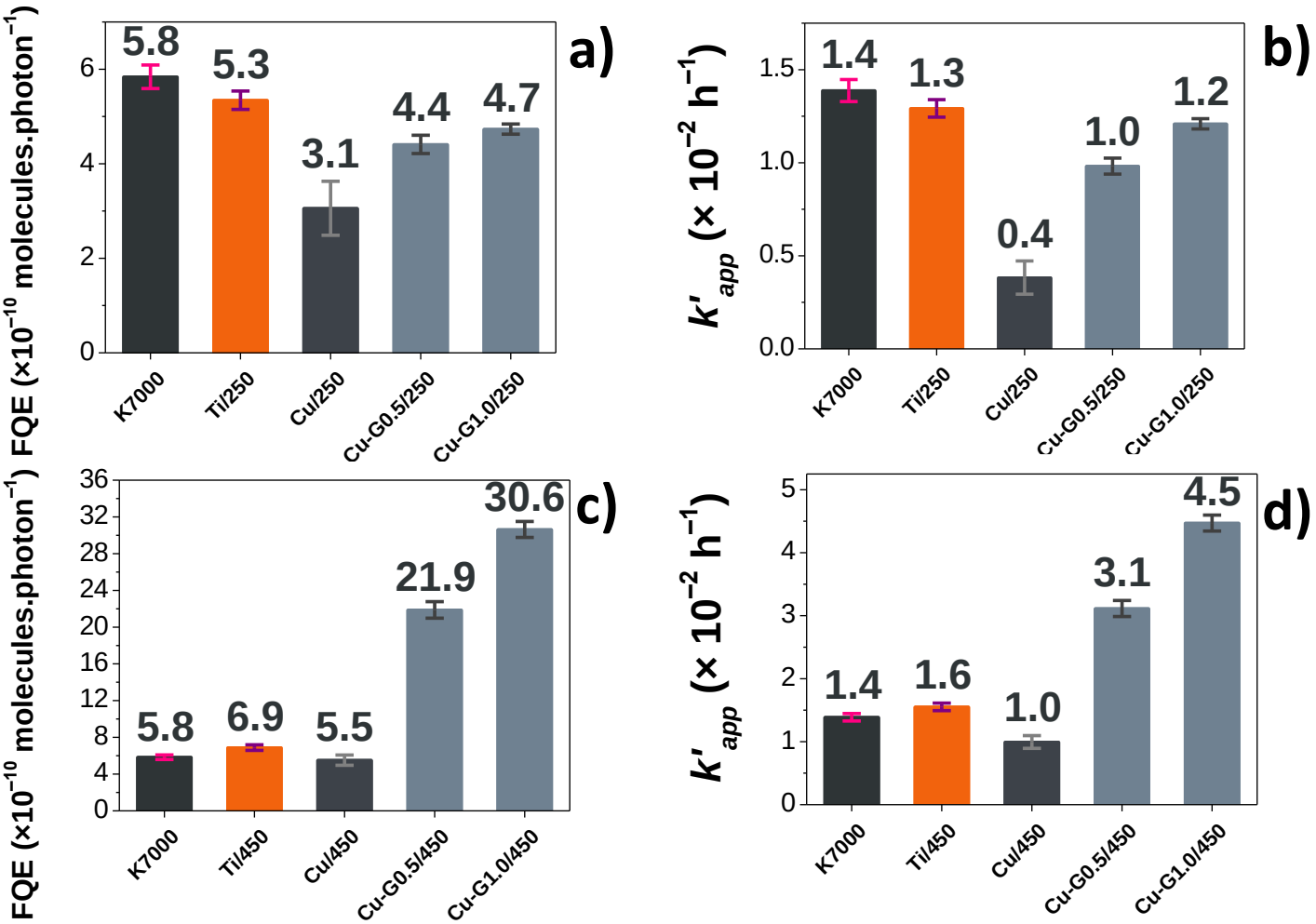

Figure 5. Histograms depicting the FQE rates of prepared photocatalysts for benzene removal using the white light LED lamp, for a total reaction time of 5 h. a), and c): specimens thermally treated at 250 °C / 8 h, and 450 °C / 2h, respectively.
Histograms showing the pseudo-first order kinetic constants (first 1 h reaction), k'_{app}. b), and d): specimens thermally treated at 250 °C / 8 h, and 450 °C / 2h, respectively. Reported values are averaged over three consecutive photocatalytic benzene removal tests. The error bars represent the standard error over three photocatalytic experiments.

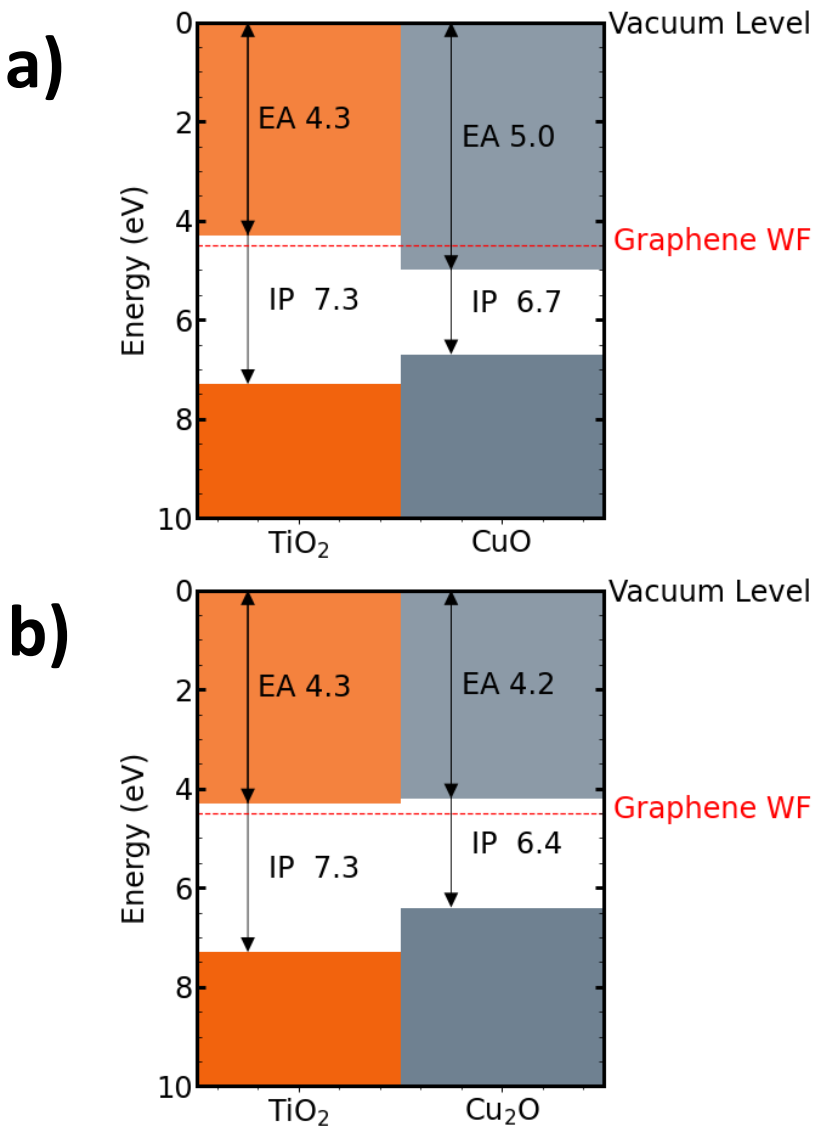

Figure 6. Type-I band alignment for TiO_2-CuO heterojunction (a), and type-II staggered heterojunction for TiO_2-Cu_2O (b) shown with respect to the WF of graphene. Energy levels of TiO_2, CuO, and Cu_2O are from Xu and Schoonen [31]; the value for graphene WF is from Liang and Ang [30]. The E_g of TiO_2 is from specimen **Cu-G1.0/450**. EA and IP stand for electron affinity, and ionisation potential, respectively.
Plots drawn with the MacroDensity python script [32].

An (qualitative and quantitative) identification of all of the intermediates of benzene photocatalytic oxidation is well beyond the scope of this work. However, with the available experimental data, together with the support of previous literature, we could speculate about (some of) the likely photocatalytic degradation products of benzene oxidation. To this aim, we extracted (at selected irradiation times) gas-chromatograms from the gas-analyser during the photocatalytic experiments – specimen **Cu-G1.0/450**, shown in Figure S3. At time zero, just before switching the white-light LED lamp on, benzene is virtually the only species inside the reacting system (Figure S3a). Once the white LED has been turned on, the photocatalytic reaction started,

so much so at time t = 0.5 h, the concentration of benzene decreased, and degradation compounds lighter than benzene, started appearing (Figure S3b). The molar mass of benzene is M = 78.11 g.mol^{-1}. A recent work by Chen *et al*., by means of *in-situ* diffuse reflectance infrared Fourier transform spectroscopy over $ZnWO_4$ nanorods, proposed methylene (CH_2, M = 14.03 g.mol^{-1}), coming from the breaking of the aromatic ring, as a possible initial degradation by-product of benzene photocatalytic oxidation [33]. Ollis and co-authors, by means of GC/MS analysis, found carboxylic acids – acetic and formic acid (M = 60.05, and 46.03 g.mol^{-1}, respectively) – as intermediates of benzene photocatalytic oxidation over TiO_2 [34]. Thus, the presence of those intermediates is reasonable here. At t = 2 h, and t = 4 h irradiation time (Figure S3c,d), there is an increase in concentration of lighter degradation compounds of benzene. As a result, it is evident that different reaction conditions give different reaction mechanisms/paths for the gas-phase photocatalytic oxidation of benzene [35]. Yet, a real application requires a stable reuse of the photocatalytic material. Stability of **Cu-G1.0/450** over three consecutive photocatalytic runs is displayed in Figure S4.

2.2.2 NO_x abatement

Given the benzene removal photocatalytic results, de-NO_x tests were carried out only with the specimens thermally treated at 450 °C / 2h. Results are reported in Figure 7a-d. A photocatalytic de-NO_x plot is displayed in Figure S5. **Cu-G1.0/450** confirmed to be the most active (under white-light exposure) photocatalyst, with a FQE value of 3.3×10^{-3} molecules.photon^{-1} that is more than twice the removal rate of the commercial anatase-based photocatalyst (**K7000**, FQE = 1.5×10^{-3} molecules.photon^{-1}), Figure 7a. Indeed, all of the synthesised photocatalysts were shown to be more active than K7000 – unmodified **Ti/450**, being a mixture of anatase and rutile TiO_2 polymorphs has been shown to be photocatalytically active against isopropanol degradation [15]. [Anatase and rutile, also as nanoparticles [36], when in form of a heterojunction are able to absorb visible light [37].] Those results are confirmed by the initial (first 2 min of reaction) pseudo-first order kinetic constant k'_{app} data, reported in Figure 7b. **Cu-G1.0/450** was that having the higher initial de-NO_x rate, this being equal to 6.8×10^{-2} h^{-1} (*versus* 5.4×10^{-2} h^{-1} of **Cu-G0.5/450**). This is more than twice as higher than the k'_{app} rate constant of unmodified titanias (**K7000** = 3.1×10^{-2} h^{-1}; **Ti/450** = 2.9×10^{-2} h^{-1}). However, for a photocatalyst to be effective in NO_x removal, parameters as selectivity for the formation of ionic species and conversion of NO are also important, as NO_2 is more hazardous to human beings than NO [38]. If from the one hand all of the tested photocatalysts showed to possess very good selectivity toward the formation of ionic species (values ranging from 91% in **Cu-G0.5/450** to 100% in **K7000**, Figure 7c), from the other, **Cu-G1.0/450** was that showing the highest NO conversion percentages amongst the whole series, 24% against 9% of **K7000**, Figure 7d. Thus, TiO_2 surface modification with 1mol% CuxO, and 1 wt% graphene (**Cu-G1.0/450**) showed promise to de-NO_x properties, limiting the formation of NO_2, and improving the selectivity to the reaction for N_2 evolution. Furthermore, similarly to the benzene removal photocatalytic tests, **Cu-G1.0/450** proved itself to be recyclable also in consecutive photocatalytic experiments, as displayed in Figure

S6. Moreover, with the available data, we can fairly speculate that NO_x abatement mainly followed the NO oxidation path by $O_2^{\bullet-}$ species (formed by the photogenerated electrons in reductive reactions with oxygen from the environment) [39].

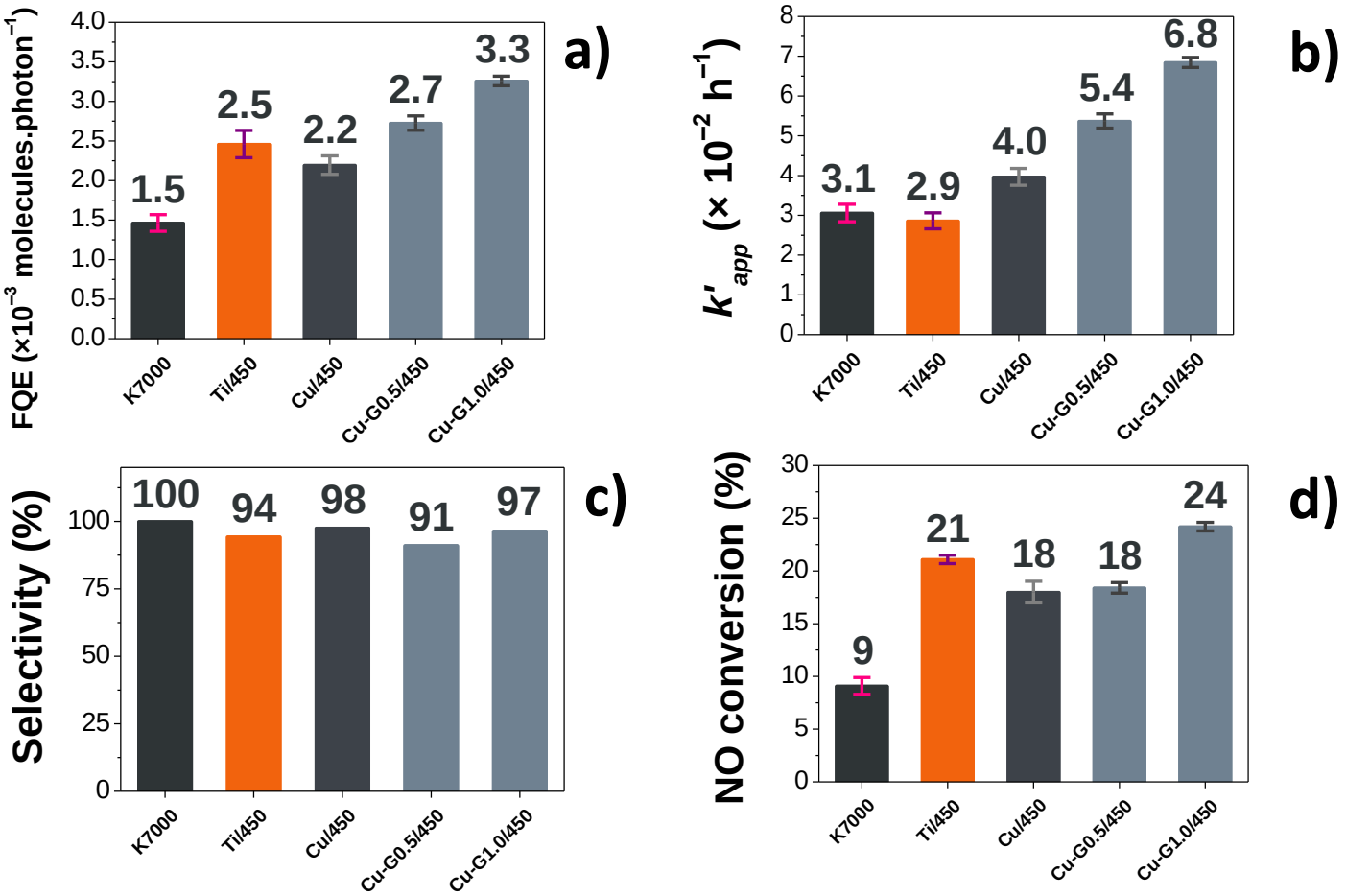

Figure 7. Histograms showing the de-NO_x results in terms of: a) FQE, for a total reaction time of 10 min; b) first 2 min of reaction pseudo-first order kinetic constants, k'_{app}; c) selectivity (%) for the formation of ionic species; d) NO conversion (%). The error bars represent the standard error over three photocatalytic experiments.

The generation of superoxide anion upon light exposure has been detected *via* indirect EPR spin trapping technique utilising 5,5'-dimethyl-1-pyrroline *N*-oxide (DMPO) as a spin trap in photocatalyst's DMSO suspensions in the presence of molecular oxygen. Exposure to light of the reacting system (*i.e.*: photocatalyst/DMPO/DMSO/air) led to the formation of four spin-adducts: DMPO-$O_2^{\bullet-}$, DMPO-$OCH_3^{\bullet}$, along with DMPO-$OR^{\bullet}$ and DMPO-$CH_3^{\bullet}$. Figure 8 shows the EPR spectrum of **Cu-G1.0/450/DMPO/DMSO/air** upon 10-minutes light exposure, along with their spin Hamiltonian parameters, which were obtained from the simulation analysis. The superoxide anion has been detected, as its corresponding spin-adduct was the main species produced upon exposure (relative concentration ~70%), and it has been formed by the reaction of photogenerated electron with molecular oxygen. Methoxy radical originates from the DMSO solvent, which reacts with reactive oxygen species ($O_2^{\bullet-}$/$OOH^{\bullet}$ or $HO^{\bullet}$) to form the methyl radical and its subsequent transformation in a process of rapid reactions with DMPO and molecular oxygen to DMPO-$OCH_3^{\bullet}$ (relative

concentration ~13%) [40]. Methyl radical may also be detected, depending on the reaction condition, as DMPO-$OCH_3^{\bullet}$ spin-adduct (relative concentration: 7%). The oxygen-centred spin-adduct DMPO-$OR^{\bullet}$ (relative concentration ~10%) comes from the decomposition of DMSO solvent [40]. The intensity of the EPR signal reflected the character of photocatalyst, the highest signal was monitored for reaction systems with **Ti/450**, for the copper- and copper-graphene-decorated titania materials intensity was lower due to electron transfer to CuO conduction band and reduction of Cu(II).

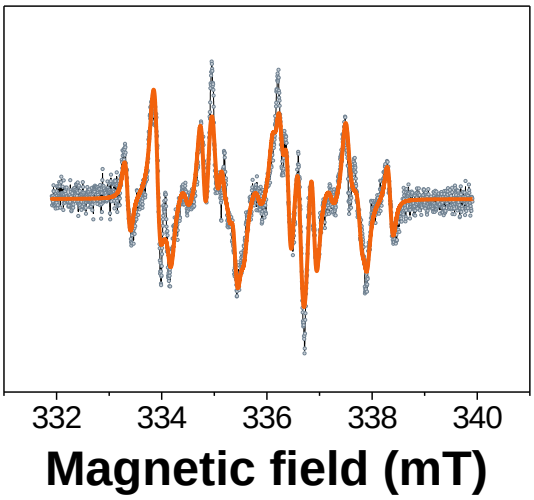

Spin-adduct	Hyperfine coupling constants (mT)		*g*-value
	a_N	a_i	
DMPO-$O_2^{\bullet-}$	1.286	a_H^{β} = 1.038 a_H^{γ} = 0.133	2.0057
DMPO-$OCH_3^{\bullet}$	1.345	a_H^{β} = 0.832 a_H^{γ} = 0.173	2.0057
DMPO-$OR^{\bullet}$	1.261	a_H^{β} = 1.455	2.0057
DMPO-$CH_3^{\bullet}$	1.464	a_H^{β} = 2.082	2.0058

Figure 8. Experimental (blue circles) and simulated (continuous orange line) EPR spectrum (SW = 8 mT) obtained after continuous exposure (LED@365 nm, dose 4.8 J.cm^{-2}), specimen **Cu-G1.0/450** in DMSO (c_0 = 0.80 mg.mL^{-1}), in the presence of DMPO (c_0 = 0.04 M) and air, along with hyperfine coupling constants, and *g*-value.

3. Conclusions

As human beings spend the majority of their time indoors, good indoor air quality standards should be guaranteed worldwide. However, poor indoor air causes several adverse health effects and thus should be treated as a global interest. Photocatalysis might be a partial response to such a concern. To this aim, we have synthesised, by means of a green, clean, and simple sol–gel method, titania modified with copper oxide(s) and graphene hybrid nanomaterials. Photocatalytic activity of as-prepared materials was tested against two class of pollutants commonly found indoor: benzene as model volatile organic compound, and nitrogen oxides. A white-light LED bulb commonly found inside households was employed as the light source. We have shown that copper species allowed for the absorption of visible-light. Furthermore, upon visible-light exposure, Cu(II) is continuously reduced to Cu(I), allowing for the formation of TiO_2-Cu_2O junction, favouring the separation of the photogenerated exciton. Addition of graphene enhanced that electron mobility, decreasing the recombination rate of the photogenerated exciton. EPR spectroscopy confirms the reduction of Cu(II) to Cu(I), as well as the generation of reactive oxygen species (mainly superoxide radical anions) upon light exposure. Results showed that the addition of 1 mol% Cu_xO together with 1.0 wt% of

graphene to TiO_2 enabled up to a three-fold increase in the photocatalytic removal of those gaseous pollutants, compared to unmodified titania and to a commercially available TiO_2. Prepared photocatalysts were also shown to be fully recyclable over repeated tests. This makes our material a suitable candidate for improving households' indoor air quality.

Acknowledgements

This work was partly developed within the scope of the bilateral project between Portugal and the Slovak Republic, FCT/484/January 15, 2019/S, and in the frame of the project CICECO–Aveiro Institute of Materials, UIDB/50011/2020 & UIDP/50011/2020, financed by national funds through the Portuguese Foundation for Science and Technology/MCTES. This research was also partly financially supported by the Scientific Grant Agency of the Slovak Republic (VEGA Project 1/0064/21), and Slovak Research and Development Agency under the contract No. SK-PT-2018-0007. David Maria Tobaldi thanks FCT and Portuguese national funds (OE), through FCT, I.P., in the scope of the framework contract foreseen in the numbers 4, 5 and 6 of the article 23, of the Decree-Law 57/2016, of August 29, changed by Law 57/2017, of July 19. Luc Lajaunie gratefully acknowledges the support from the acknowledges funding from the Andalusian regional government (FEDER-UCA-18-106613), and that of the Spanish Ministerio de Economia y Competitividad (PID2019-107578GA-I00). This project has also received partial funding from the European Union's Horizon 2020 research and innovation programme under grant agreement No 823717 – ESTEEM3. Dana Dvoranová thanks the Ministry of Education, Science, Research and Sport of the Slovak Republic for funding within the scheme "*Excellent research teams*". Prof Vlasta Brezová (Slovak University of Technology in Bratislava) is heartfully acknowledged for the fruitful discussion. Last but not less important, we are very much obliged to Miss Dafne Maria Glaglanon for proof-editing the English of the manuscript.

References

[1] N.E. Klepeis, W.C. Nelson, W.R. Ott, J.P. Robinson, A.M. Tsang, P. Switzer, J.V. Behar, S.C. Hern, W.H. Engelmann, The National Human Activity Pattern Survey (NHAPS): a resource for assessing exposure to environmental pollutants, J. Expo. Sci. Environ. Epidemiol. 11 (2001) 231–252. https://doi.org/10.1038/sj.jea.7500165.

[2] O. US EPA, Indoor Air Quality, US EPA. (2017). https://www.epa.gov/report-environment/indoor-air-quality

[3] I.C. Dedoussi, S.D. Eastham, E. Monier, S.R.H. Barrett, Premature mortality related to United States cross-state air pollution, Nature. 578 (2020) 261–265. https://doi.org/10.1038/s41586-020-1983-8.

[4] W. Du, G. Wang, Indoor Air Pollution was Nonnegligible during COVID-19 Lockdown, Aerosol Air Qual. Res. 20 (2020) 1851–1855. https://doi.org/10.4209/aaqr.2020.06.0281.

[5] G. Liu, M. Xiao, X. Zhang, C. Gal, X. Chen, L. Liu, S. Pan, J. Wu, L. Tang, D. Clements-Croome, A review of air filtration technologies for sustainable and healthy building ventilation, Sustain. Cities Soc. 32 (2017) 375–396. https://doi.org/10.1016/j.scs.2017.04.011.
[6] H. Ren, P. Koshy, W.-F. Chen, S. Qi, C.C. Sorrell, Photocatalytic materials and technologies for air purification, J. Hazard. Mater. 325 (2017) 340–366. https://doi.org/10.1016/j.jhazmat.2016.08.072.
[7] A. Fujishima, T.N. Rao, D.A. Tryk, Titanium dioxide photocatalysis, J. Photochem. Photobiol. C Photochem. Rev. 1 (2000) 1–21. https://doi.org/10.1016/S1389-5567(00)00002-2.
[8] Commission Regulation (EC) No 244/2009 of 18 March 2009 implementing Directive 2005/32/EC of the European Parliament and of the Council with regard to ecodesign requirements for non-directional household lamps (Text with EEA relevance), 2009. http://data.europa.eu/eli/reg/2009/244/oj/eng
[9] C. Casado, R. Timmers, A. Sergejevs, C.T. Clarke, D.W.E. Allsopp, C.R. Bowen, R. van Grieken, J. Marugán, Design and validation of a LED-based high intensity photocatalytic reactor for quantifying activity measurements, Chem. Eng. J. 327 (2017) 1043–1055. https://doi.org/10.1016/j.cej.2017.06.167.
[10] L. Da Vià, C. Recchi, E.O. Gonzalez-Yañez, T.E. Davies, J.A. Lopez-Sanchez, Visible light selective photocatalytic conversion of glucose by TiO_2, Appl. Catal. B Environ. 202 (2017) 281–288. https://doi.org/10.1016/j.apcatb.2016.08.035.
[11] A.M. Ferrari-Lima, R.P. de Souza, S.S. Mendes, R.G. Marques, M.L. Gimenes, N.R.C. Fernandes-Machado, Photodegradation of benzene, toluene and xylenes under visible light applying N-doped mixed TiO_2 and ZnO catalysts, Catal. Today. 241 (2015) 40–46. https://doi.org/10.1016/j.cattod.2014.03.042.
[12] S. Douven, J.G. Mahy, C. Wolfs, C. Reyserhove, D. Poelman, F. Devred, E.M. Gaigneaux, S.D. Lambert, Efficient N, Fe Co-Doped TiO_2 Active under Cost-Effective Visible LED Light: From Powders to Films, Catalysts. 10 (2020) 547. https://doi.org/10.3390/catal10050547.
[13] Y. Liu, J. Liu, Y. Lin, Y. Zhang, Y. Wei, Simple fabrication and photocatalytic activity of S-doped TiO_2 under low power LED visible light irradiation, Ceram. Int. 35 (2009) 3061–3065. https://doi.org/10.1016/j.ceramint.2009.04.021.
[14] V. Vaiano, O. Sacco, G. Iervolino, D. Sannino, P. Ciambelli, R. Liguori, E. Bezzeccheri, A. Rubino, Enhanced visible light photocatalytic activity by up-conversion phosphors modified N-doped TiO_2, Appl. Catal. B Environ. 176–177 (2015) 594–600. https://doi.org/10.1016/j.apcatb.2015.04.049.
[15] D.M. Tobaldi, L. Lajaunie, N. Rozman, A.P.F. Caetano, M.P. Seabra, A. Sever Škapin, R. Arenal, J.A. Labrincha, Impact of the absolute rutile fraction on TiO_2 visible-light absorption and visible-light-promoted photocatalytic activity, J. Photochem. Photobiol. Chem. 382 (2019) 111940. https://doi.org/10.1016/j.jphotochem.2019.111940.
[16] P.A. Ochoa Rodríguez, S.G. Casuscelli, V.R. Elías, G.A. Eimer, LED visible-light activated mesoporous TiO_2: A better understanding about carbon role in the photocatalytic performance of solid, Catal. Today. (2020). https://doi.org/10.1016/j.cattod.2020.10.015.
[17] D.M. Tobaldi, L. Lajaunie, D. Dvoranová, V. Brezová, B. Figueiredo, M.P. Seabra, J.J. Calvino, J.A. Labrincha, Cooperative and fully reversible color switching activation in hybrid graphene decorated nanocages and copper-TiO_2 nanoparticles, Mater. Today Energy. 17 (2020) 100460. https://doi.org/10.1016/j.mtener.2020.100460.
[18] L. Lajaunie, C. Pardanaud, C. Martin, P. Puech, C. Hu, M.J. Biggs, R. Arenal, Advanced spectroscopic analyses on a:C-H materials: Revisiting the EELS characterization and its coupling with multi-wavelength Raman spectroscopy, Carbon. 112 (2017) 149–161. https://doi.org/10.1016/j.carbon.2016.10.092.
[19] R.G. Burns, Mineralogical Applications of Crystal Field Theory, Cambridge University Press, 1993.
[20] F.C. Hawthorne, Mineralogical Society of America, eds., Spectroscopic methods in mineralogy and geology, Mineralogical Society of America, Washington, D.C., 1988.
[21] H. Irie, K. Kamiya, T. Shibanuma, S. Miura, D.A. Tryk, T. Yokoyama, K. Hashimoto, Visible Light-Sensitive Cu(II)-Grafted TiO_2 Photocatalysts: Activities and X-ray Absorption Fine Structure Analyses, J. Phys. Chem. C. 113 (2009) 10761–10766. https://doi.org/10.1021/jp903063z.

[22] Q. Huang, S. Tian, D. Zeng, X. Wang, W. Song, Y. Li, W. Xiao, C. Xie, Enhanced Photocatalytic Activity of Chemically Bonded TiO_2/Graphene Composites Based on the Effective Interfacial Charge Transfer through the C–Ti Bond, ACS Catal. 3 (2013) 1477–1485. https://doi.org/10.1021/cs400080w.
[23] S. Banerjee, D. Chakravorty, Optical absorption by nanoparticles of Cu_2O, Europhys. Lett. EPL. 52 (2000) 468–473. https://doi.org/10.1209/epl/i2000-00461-5.
[24] T. Zhu, S.-P. Gao, The Stability, Electronic Structure, and Optical Property of TiO_2 Polymorphs, J. Phys. Chem. C. 118 (2014) 11385–11396. https://doi.org/10.1021/jp412462m.
[25] D.M. Tobaldi, D. Dvoranová, L. Lajaunie, N. Rozman, B. Figueiredo, M.P. Seabra, A.S. Škapin, J.J. Calvino, V. Brezová, J.A. Labrincha, Graphene-TiO_2 hybrids for photocatalytic aided removal of VOCs and nitrogen oxides from outdoor environment, Chem. Eng. J. 405 (2021) 126651. https://doi.org/10.1016/j.cej.2020.126651.
[26] M.D. Ward, J.R. White, A.J. Bard, Electrochemical investigation of the energetics of particulate titanium dioxide photocatalysts. The methyl viologen-acetate system, J. Am. Chem. Soc. 105 (1983) 27–31. https://doi.org/10.1021/ja00339a007.
[27] Z. Barbieriková, D. Dvoranová, M.-V. Sofianou, C. Trapalis, V. Brezová, UV-induced reactions of Mg^{2+} -doped anatase nanocrystals with exposed {0 0 1} facets: An EPR study, J. Catal. 331 (2015) 39–48. https://doi.org/10.1016/j.jcat.2015.08.009.
[28] V. Brezová, D. Dvoranová, A. Staško, Characterization of titanium dioxide photoactivity following the formation of radicals by EPR spectroscopy, Res. Chem. Intermed. 33 (2007) 251–268. https://doi.org/10.1163/156856707779238630.
[29] D.M. Tobaldi, K. Kočí, M. Edelmannová, L. Lajaunie, B. Figueiredo, J.J. Calvino, M.P. Seabra, J.A. Labrincha, Cu_xO and carbon–modified TiO_2–based hybrid materials for photocatalytically assisted H_2 generation, Mater. Today Energy. 19 (2021) 100607. https://doi.org/10.1016/j.mtener.2020.100607.
[30] S.-J. Liang, L.K. Ang, Electron Thermionic Emission from Graphene and a Thermionic Energy Converter, Phys. Rev. Appl. 3 (2015) 014002. https://doi.org/10.1103/PhysRevApplied.3.014002.
[31] Y. Xu, M.A.A. Schoonen, The absolute energy positions of conduction and valence bands of selected semiconducting minerals, Am. Mineral. 85 (2000) 543–556.
[32] Keeeto, A. Walsh, Jarvist Moore Frost, Wmd-Group/Macrodensity: Macroback, Zenodo, 2017. https://doi.org/10.5281/ZENODO.884521.
[33] D. Ma, L. Yang, Z. Sheng, Y. Chen, Photocatalytic degradation mechanism of benzene over $ZnWO_4$: Revealing the synergistic effects of Na-doping and oxygen vacancies, Chem. Eng. J. 405 (2021) 126538. https://doi.org/10.1016/j.cej.2020.126538.
[34] O. d'Hennezel, P. Pichat, D.F. Ollis, Benzene and toluene gas-phase photocatalytic degradation over H_2O and HCL pretreated TiO_2: by-products and mechanisms, J. Photochem. Photobiol. Chem. 118 (1998) 197–204. https://doi.org/10.1016/S1010-6030(98)00366-9.
[35] V. Augugliaro, M. Bellardita, V. Loddo, G. Palmisano, L. Palmisano, S. Yurdakal, Overview on oxidation mechanisms of organic compounds by TiO_2 in heterogeneous photocatalysis, J. Photochem. Photobiol. C Photochem. Rev. 13 (2012) 224–245. https://doi.org/10.1016/j.jphotochemrev.2012.04.003.
[36] C. Maheu, L. Cardenas, E. Puzenat, P. Afanasiev, C. Geantet, UPS and UV spectroscopies combined to position the energy levels of TiO_2 anatase and rutile nanopowders, Phys. Chem. Chem. Phys. 20 (2018) 25629–25637. https://doi.org/10.1039/C8CP04614J.
[37] D.O. Scanlon, C.W. Dunnill, J. Buckeridge, S.A. Shevlin, A.J. Logsdail, S.M. Woodley, C.R.A. Catlow, M.J. Powell, R.G. Palgrave, I.P. Parkin, G.W. Watson, T.W. Keal, P. Sherwood, A. Walsh, A.A. Sokol, Band alignment of rutile and anatase TiO_2, Nat. Mater. 12 (2013) 798–801. https://doi.org/10.1038/nmat3697.
[38] J. Ângelo, L. Andrade, L.M. Madeira, A. Mendes, An overview of photocatalysis phenomena applied to NOx abatement, J. Environ. Manage. 129 (2013) 522–539. https://doi.org/10.1016/j.jenvman.2013.08.006.
[39] J. Lasek, Y.-H. Yu, J.C.S. Wu, Removal of NO_x by photocatalytic processes, J. Photochem. Photobiol. C Photochem. Rev. 14 (2013) 29–52. https://doi.org/10.1016/j.jphotochemrev.2012.08.002.

[40] D. Dvoranová, Z. Barbieriková, V. Brezová, Radical Intermediates in Photoinduced Reactions on TiO2 (An EPR Spin Trapping Study), Molecules. 19 (2014) 17279–17304. https://doi.org/10.3390/molecules191117279.